IOP Publishing Smart Materials and Structures
Smart Mater. Struct. **26** (2017) 115022 (11pp) https://doi.org/10.1088/1361-665X/aa8f71

Structural parameter study on polymer-based ultrasonic motor

Jiang Wu, Yosuke Mizuno and Kentaro Nakamura

Laboratory for Future Interdisciplinary Research of Science and Technology, Tokyo Institute of Technology, Yokohama 226-8503, Japan

E-mail: wujiang@sonic.pi.titech.ac.jp

Received 21 June 2017, revised 21 August 2017
Accepted for publication 27 September 2017
Published 20 October 2017

Abstract

Our previous study has shown that traveling-wave rotary ultrasonic motors using polymer-based vibrators can work in the same way as conventional motors with metal-based vibrators. It is feasible to enhance the performance, particularly output torques, of polymer-based motors by adjusting several key dimensions of their vibrators. In this study, poly phenylene sulfide, a functional polymer exhibiting low attenuation at ultrasonic frequency, is selected as the vibrating body, which is activated with a piezoelectric ceramic element bonded on its back surface. The optimal thicknesses of the polymer-based motors are higher than those of metal-based motors. When the same voltages were applied, the maximum torques and output powers available with the polymer-based motors were lower than the values of the metal-based motors with the same structures. The reasons for the lower torque were explained on the basis of vibration modes. First, the force factors of the polymer-based vibrators are lower than those of metal-based vibrators owing to the great difference in the mechanical constants between polymers and piezoelectric ceramics. Subsequently, though the force factors of polymer-based vibrators can be slightly enhanced by increasing their thicknesses, the unavoidable radial vibrations become higher and cause undesirable friction loss, which reduces the output torques. Though the polymer-based motors have rotation speeds comparable to those of metal-based motors, their output power are lower due to the low electromechanical coupling factors of the polymer-based vibrators.

Keywords: elliptical motion, force factor, polymer, ultrasonic motor

(Some figures may appear in colour only in the online journal)

1. Introduction

Ultrasonic motors (USMs), which provide relatively low speeds, high torques, and quick responses, compared to the electro-magnetic motors, have been practically applied to a part of cameras and optical instruments for over two decades [1, 2], and also expected as potential key actuators for robotics [3, 4]. In general, USM consists of a vibrator and a rotor, which are pressed to each other to effectively utilize the friction force. When two channels of voltages with a 90° phase are applied to a vibrator, a traveling wave or two degenerated standing waves are excited, and elliptical motion at vibrator surface drives the rotor [3–6]. Vibrators in the conventional USMs were commonly composed of piezoelectric ceramics and a metal vibrating body [7–11]. Recently, light USMs have become increasingly demanded [12]. In our previous study, metals were replaced with functional polymers as vibrating bodies of USMs to reduce their weight and enhance the mass production efficiencies [12–15]. Poly phenylene sulfide (PPS) was selected due to its low damping coefficient of 0.0025, which is 0.05 and 2 times the values for acrylic resin and stainless steel, respectively, under high-amplitude vibration (up to 0.04% strain) [12, 14]. We fabricated a PPS-based ring-shaped vibrator to form a traveling-wave rotary USM, and tested its performance [15]. Compared to the metal-based USMs, the PPS-based USM provided relatively high rotation speed but low output torque. As PPS exhibits a much lower elastic modulus and density than metals, the optimal design of PPS-based USMs should differ from those of metal-based ones.

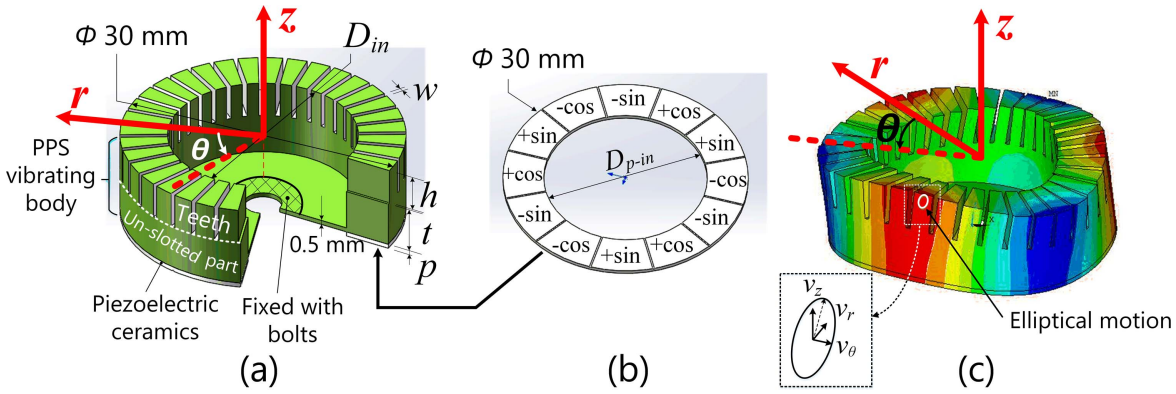

Figure 1. (a) Vibrator structure, (b) electrode division of piezoelectric ceramic element, and (c) the 3rd bending mode and elliptical motion at vibrator surface.

Table 1. Mechanical constants of polymer, metals, and piezoelectric ceramics.

Material		Density ($\times 10^3$ kg m^{-3})	Elastic modulus (GPa)	Poisson's ratio
Polymer:	PPS	1.35	3.45	0.36
Metals:	Copper alloy	8.50	117	0.31
	Aluminum alloy	2.70	70.3	0.35
	Stainless steel	7.90	197	0.31
Piezoelectric ceramics		7.80	145 (Y_{11})	—

In this paper, first, we explore how elliptical shapes and force factors of the polymer-based vibrators vary as several key structural parameters are changed. Subsequently, we attempt to improve the maximum torques (output torque at zero revolution speed) of the polymer-based USMs by adjusting several key dimensions, and discuss the reason for their relatively low output torques and power compared to the metal-based USMs.

2. Configuration of USM and shape parameters

Figure 1(a) depicts the configuration of the vibrator, which consists of a PPS vibrating body and a piezoelectric ceramic element. The vibrating body had a 30 mm diameter cylindrical part and a 0.5 mm thick bottom disk. Radial slots were fabricated on the cylindrical part with an interval of 10°. The vibrator has following shape parameters: the un-slotted part thickness t, the teeth height h, the thickness of piezoelectric ceramic plate p, the inner diameter of the cylindrical part D_{in}, and the slot width w. A central hole was made on the bottom disk to fix the vibrator to a shaft with two bolts. The mechanical constants of PPS are listed in table 1. A polar coordinate (z, θ, and r axes) is set on the top surface of the vibrator. The piezoelectric ceramic annular disk (C213, Fuji Ceramics, Fujinomiya, Japan) had the inner and outer diameters of 20 and 30 mm, respectively, and a thickness of 0.5 mm. Thin silver electrodes were sintered on both sides of the piezoelectric ceramic element. As shown in figure 1(b), one side was evenly divided into 12 parts, while the other side without division was glued to the back surface of the PPS vibrating body with epoxy. When four sinusoidal voltages with phases were applied to the vibrator, a traveling wave in the 3rd bending mode shown in figure 1(c) was generated along the circumference. The vibration velocity components at the top surface of the vibrator along the z, θ, and r axes are represented by v_z, v_θ, and v_r, respectively. Ratios v_θ/v_z and v_r/v_z show elliptical motion shapes, which are altered by the vibrator dimensions [16, 17].

3. Elliptical motion shape and force factor versus structural parameters

3.1. Un-slotted part thickness

The elliptical motion shape (ratios v_θ/v_z and v_r/v_z) and the force factor of the vibrator were investigated because they are essential to USMs [1, 3]. The force factor represents the ratio of the current to the vibration velocity or equivalently the ratio of the generated force to the voltage [2, 6]. These indicators reflect the vibrator characteristics, and affect the USM performance [2, 16]. In this work, we discuss the force factor defined for the tangential vibration velocity v_θ because it is parallel to the rotation direction. The vibration velocity ratios and the force factors of the PPS-based vibrators with varying un-slotted part thicknesses were obtained through both finite element analysis (FEA) and experiments. The three orthogonal vibration

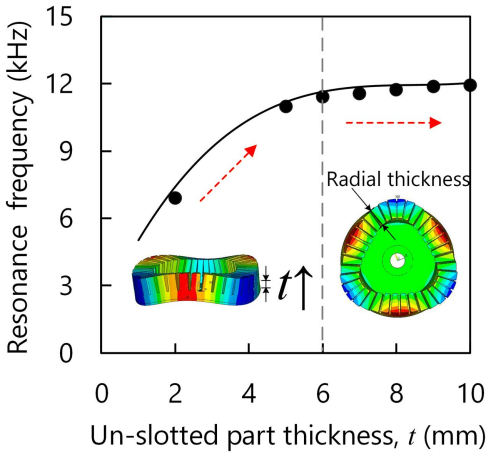

Figure 2. Simulated (lines) and experimental (dots) results of resonance frequency.

velocity components were simultaneously measured using an in-plane laser Doppler velocimeter (IPV100, Polytec, Waldbronn, Germany) and two out-of-plane laser Doppler velocimeters (CLV1000, Polytec, Waldbronn, Germany). The current was measured with a current probe (P6021, Tektronix, Beaverton, US). The vibration velocities v_z and v_r were measured at the antinodes, while the vibration velocity v_θ was at the node under the standing wave excitation. The ratios v_θ/v_z and v_r/v_z in the standing wave are exactly equal to those of the traveling wave [1].

First, we explore how the elliptical motion shape and the force factor change with varying un-slotted part thickness. The other parameters are set as $p = 0.5$ mm, $h = 4$ mm, $D_{\text{in}} = 20$ mm, and $w = 0.5$ mm. Figure 2 shows the dependence of the resonance frequency of the 3rd bending mode on the un-slotted part thickness. It increases from 5 to 11 kHz as the vibrator becomes thicker, and levels off at the un-slotted part thickness of 6 mm. For the cylindrical vibrators, the bending vibrations along the z axis couple with those along the r axis. The z-axis bending vibration is dominantly excited on the thin vibrators, and the resonance frequency increases because the equivalent stiffness becomes higher with increasing thicknesses. In contrast, the resonance frequencies on thicker vibrators are mainly determined by the radial thicknesses $D_{\text{out}}-D_{\text{in}}$ of their cylindrical parts. Figures 3(a) and (b) show the vibration velocity ratios and the force factor as a function of the un-slotted part thickness, respectively. As shown in figure 3(a), even when the vibrator became thicker, the ratio v_θ/v_z exhibited only small variation. In contrast, the ratio v_r/v_z of the vibrator with a 2 mm thick un-slotted part (t2 vibrator) was 0.7, and the value of the t10 vibrator increased to 2.8. With increasing thickness, the equivalent stiffness and mass increase, leading to the reduction in the z-axis vibration velocity [17]. However, the equivalent stiffness and mass in radial direction, determined by the radial thickness, show almost no change. Thus, the ratio v_r/v_z has an observable increase. As the un-slotted part thickness was varied from 2 to 10 mm, the force factor in figure 3(b) increased from 0.02 to 0.23 N V^{-1}. Observably, thicker vibrator generates higher force factors and higher radial vibrations.

3.2. Other shape parameters

Then, we investigated how other parameters affect the elliptical motion shapes and the force factors through FEA. Figures 4(a) and (b) show how the vibration velocity ratios and the force factors vary as the piezoelectric ceramic thicknesses p is changed, respectively. Both the ratios v_θ/v_z and v_r/v_z have little changes. When the t10 vibrators have 0.05 and 1.50 mm thick piezoelectric ceramic elements, the force factors are 0.25 and 0.28 N V^{-1}, higher than the values when the piezoelectric ceramic elements have moderate thicknesses. Figures 5(a) and (b) demonstrate how the vibration velocity ratios and the force factors depend on the teeth height h, respectively. The ratios v_θ/v_z change from 0.5 to 0.9 when the teeth heights ranged from 1 to 6 mm. With decreasing teeth height, the vibrators provide increases in the force factors and reductions in the ratio v_r/v_z. The vibration velocity ratios and the force factors are plotted as a function of the slot width w in figures 6(a) and (b), respectively. When their slots are lower than 0.5 mm, both elliptical motion shapes and force factors exhibit little changes. As shown in figures 7(a) and (b), the ratios v_θ/v_z have minimal values when the inner diameters are approximately 22 mm, where the force factors reach their peak values. The ratios v_r/v_z increase sharply as the radial thicknesses become lower. As figures 8(a) and (b) show, the optimal inner diameter is determined by the inner diameter of the piezoelectric ceramic element $D_{p\text{-in}}$, whereas the maximal force factor and the minimal ratio v_θ/v_z are independent to $D_{p\text{-in}}$. Since the un-slotted part thickness and teeth height have relatively high influences on the elliptical motion shapes and the force factors among these structural parameters, we change these parameters to improve the output torques and powers of the polymer-based USMs.

4. Performance of motors with varying dimensions

4.1. Experimental setup

In this section, we experimentally investigated how the motor performance depended on the structural parameters. Figure 9(a) illustrates the experimental setup for measuring the motor performance. The vibrator was clamped to a stainless steel shaft, fixed at the center of a stainless steel base plate. To reduce the friction loss in holding the rotor, as shown in figure 9(b), a pivot bearing composed of a conical head and a dent, both of which were made of stainless steel, was used. The conical angles of the bearing head and the dent were set to 55° and 60°, respectively. The upper shaft of the pivot bearing was inserted into a Teflon sleeve, guided along the central hole in the Teflon top plate. The dent was fixed at the center of the rotor. Preload was applied to the rotor by loading weights on the top of the shaft. As shown in figure 9(c), the rotor consisted of a contacting disk and a ring-shaped flywheel, both of which were made of aluminum. The

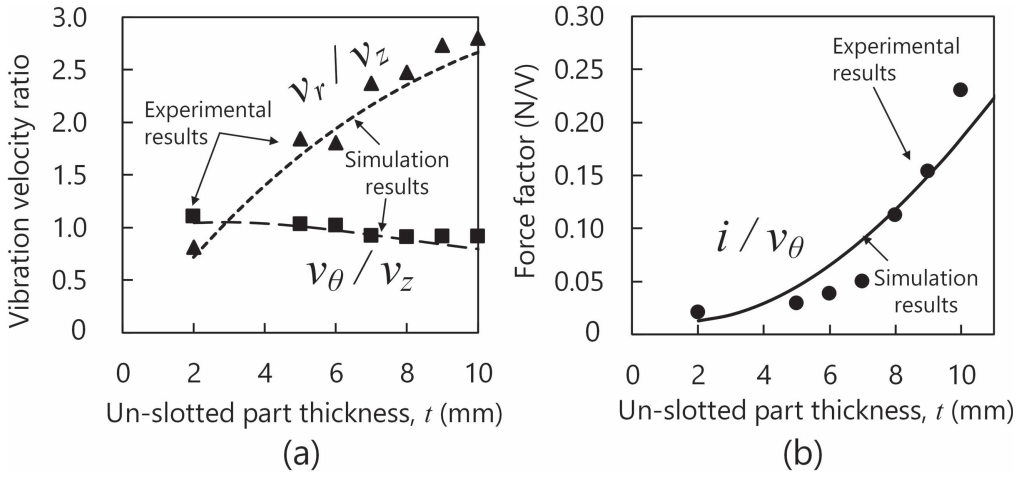

Figure 3. Simulated (lines) and experimental (dots) results of (a) elliptical motion shape and (b) force factor versus un-slotted part thickness of PPS-based vibrator.

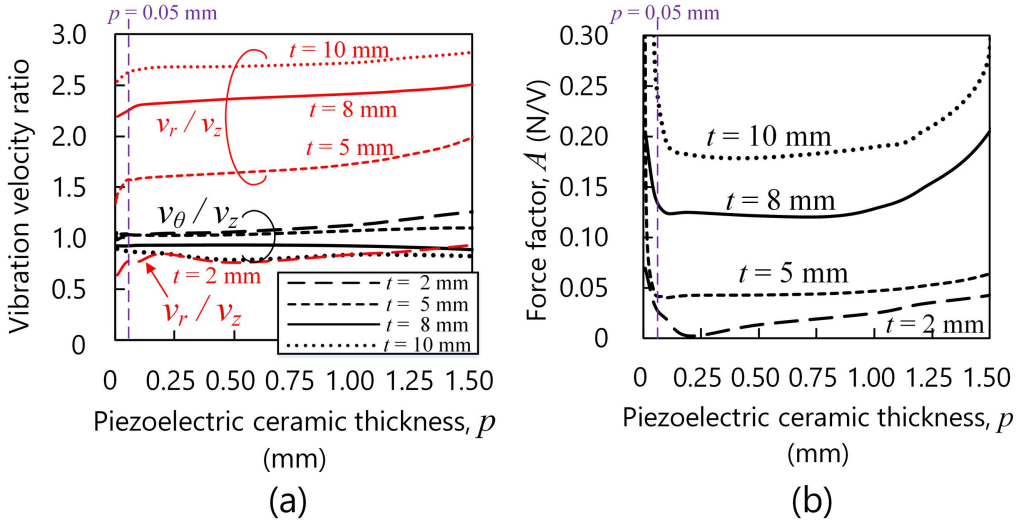

Figure 4. (a) Elliptical motion shape and (b) force factor as a function of the thickness of piezoelectric ceramics.

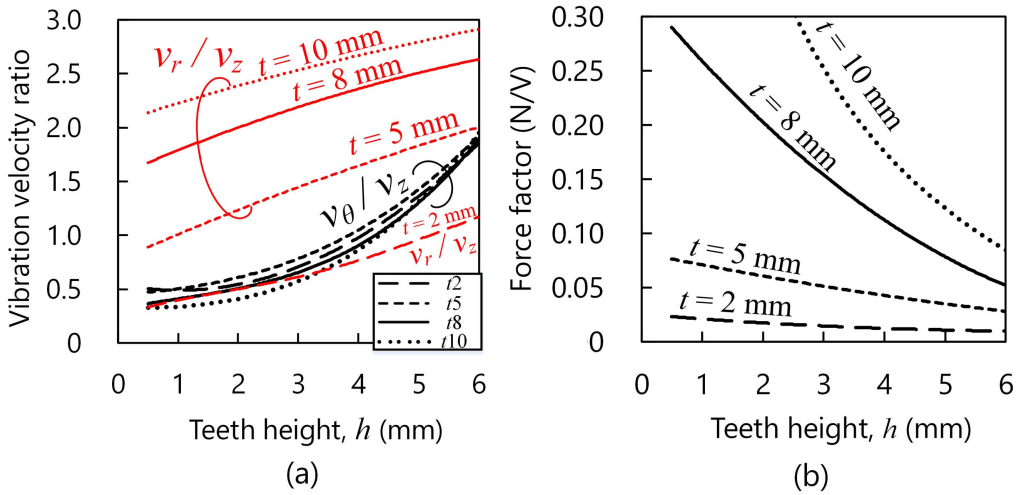

Figure 5. (a) Elliptical motion shape and (b) force factor versus slotted part thickness.

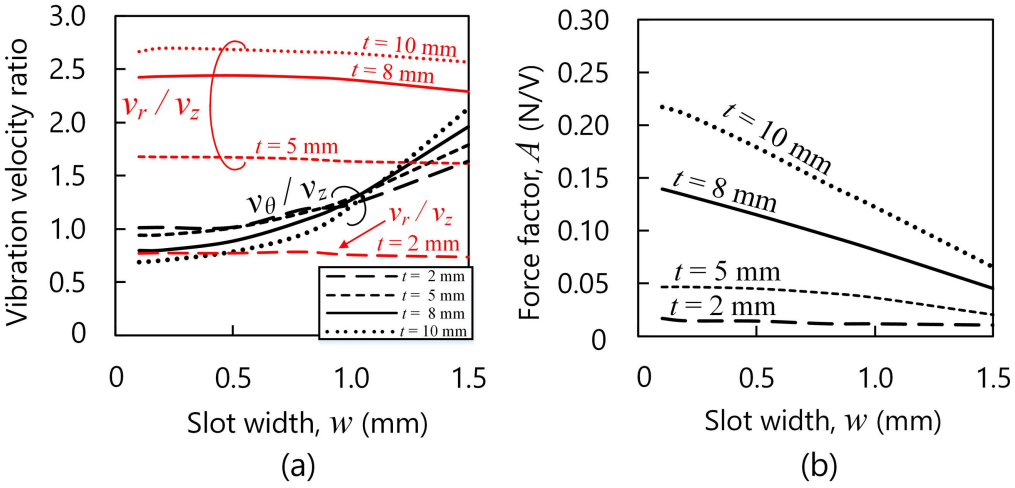

Figure 6. (a) Elliptical motion shape and (b) force factor as a function of slot width.

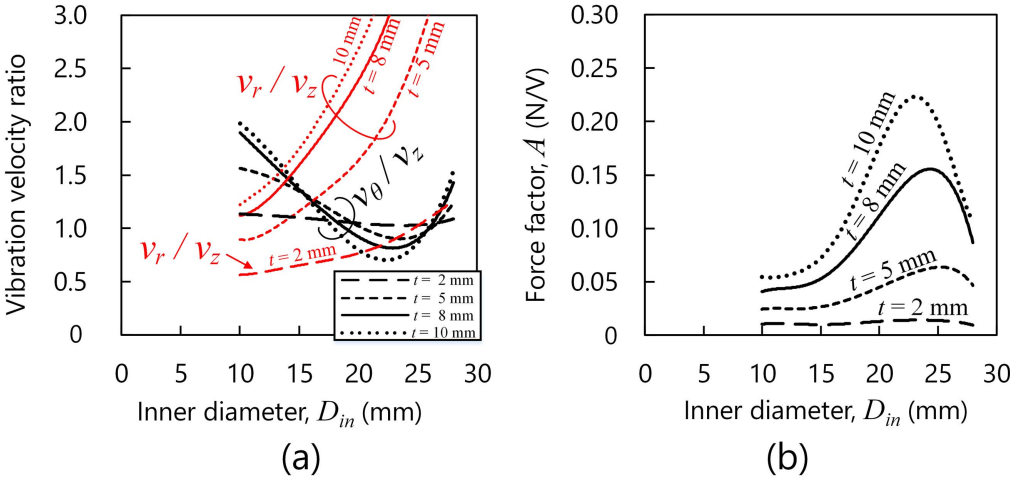

Figure 7. (a) Elliptical motion shape and (b) force factor as a function of inner diameter.

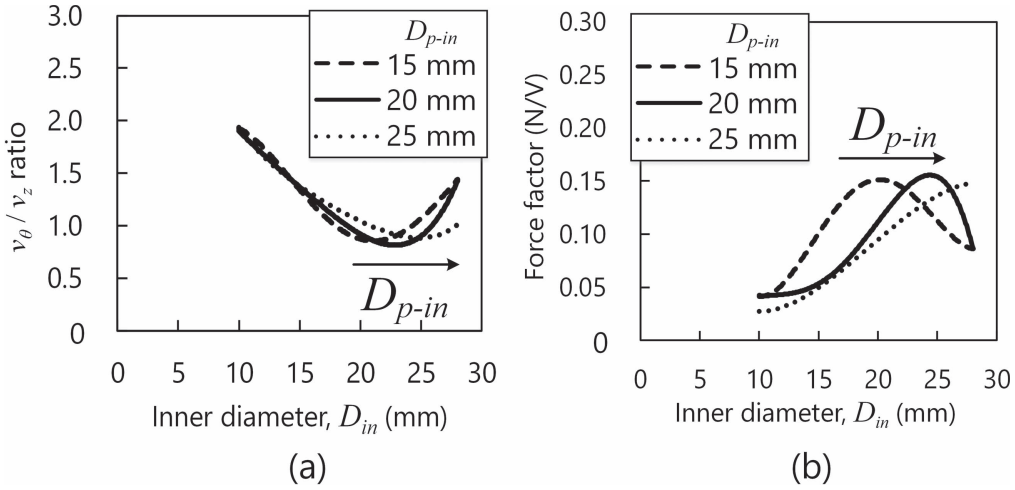

Figure 8. (a) Ratios v_θ/v_z and (b) force factors versus inner diameters of vibrators composed of piezoelectric ceramics with different inner diameters.

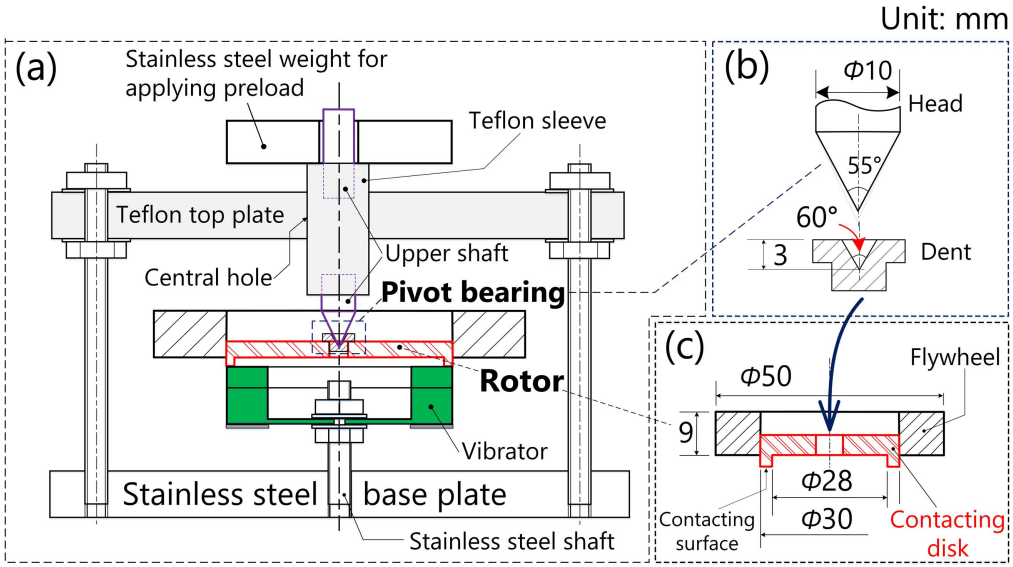

Figure 9. Testbed for evaluating motor performance. (a) Front view, (b) pivot bearing, and (c) rotor and additional flywheel.

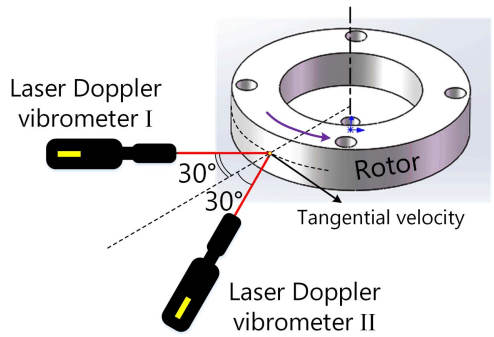

Figure 10. Rotation speed measurement with two out-of-plane laser Doppler velocimeters.

contacting surface was limited to a portion having outer and inner diameters of 30 and 28 mm, respectively, because the vibrators provided relatively extensive vibrations on the outer edges of the contacting surface (see figure 1(c)). In this study, we employed the transient method, repeatedly used in previous studies on USMs [18–20], to evaluate the motor performance. The flywheel has a moment of inertia J of 1.24×10^{-5} kg m^2. As shown in figure 10, first, the transient response of the rotor speed was measured with two out-of-plan laser Doppler velocimeters: two laser beams illuminated the same point on the outer surface of the rotor with the same angles. The tangential velocity was calculated from the outputs of the two laser Doppler velocimeters on the basis of a simple geometry [21]. Figure 11 gives an example. The measured transient response of the rotational speed of the motor with the t5 vibrator is shown in figure 11(a). The voltages and the preload are respectively 250 V and 1.04 N. Initially, the angular velocity increased from 0 to 1.21 rad s^{-1}, and leveled off at approximately 48 ms. Note that, though the angular velocity became higher in the rise part, the angular acceleration yielded a reduction. Since the lower and higher cutoff frequencies of the laser Doppler vibrometer were set to 0.2 Hz and 100 kHz, respectively, the obtained signal included ultrasonic components, which appeared to be the fluctuation in the transient response. By implementing the exponential fitting curve $\varphi(t)$ on the transient response, the maximum torque $T_{\max}$, maximum angular velocity $\varphi_{\max}$, and maximum output power $P_{\max}$ are calculated with

$$T_{\max} = J \cdot \max\left\{\frac{\mathrm{d}[\varphi(t)]}{\mathrm{d}t}\right\} = J \cdot \left.\frac{\mathrm{d}[\varphi(t)]}{\mathrm{d}t}\right|_{t=0}, \quad (1)$$

$$\varphi_{\max} = \lim_{t\to+\infty}[\varphi(t)], \quad (2)$$

and

$$P_{\max} = J \cdot \max\left\{\frac{\mathrm{d}[\varphi(t)]}{\mathrm{d}t} \cdot \varphi(t)\right\}, \quad (3)$$

respectively. As shown in figure 11(b), the motor yielded the maximum torque and angular velocity of 1.39 mNm and 1.21 rad s^{-1}, respectively, at the beginning and the end of the rise part. The maximum output power reached 0.42 mW when the motor exhibited a moderate torque.

4.2. Experimental results

Figure 12 illustrates the motor performance with the t5 vibrator as a function of the driving voltage under different preloads. As figure 12(a) shows, there existed a dead region in the maximum torque when the voltage was lower than 100–150 V. Beyond the dead region, the maximum torque increased in proportion to the driving voltage and saturated according to the preload. At a certain voltage, the maximum torque became higher with increasing preload [2]. When the preload exceeded a certain value, the maximum torque decreased because of friction loss. For example, the maximum torque at 150 V reached 0.4 mNm when the optimal preload of 0.37 N was applied to the vibrator. The maximum

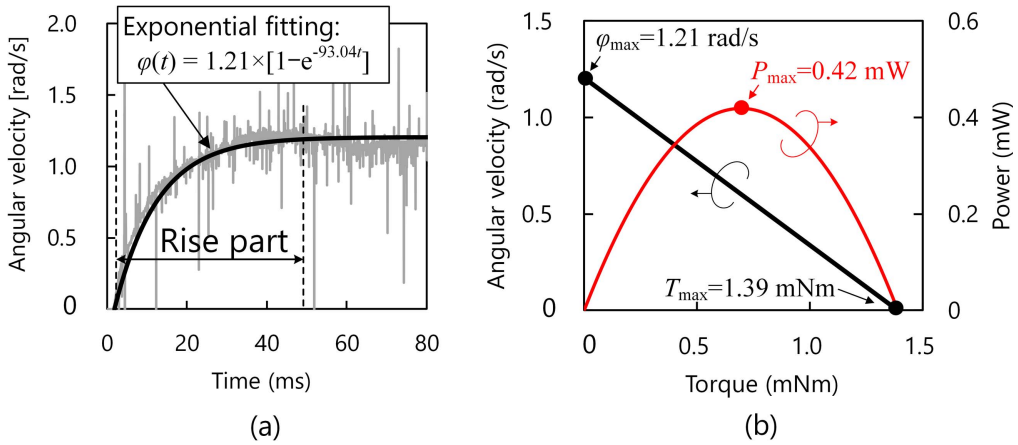

Figure 11. (a) Transient response (gray curve) of rotational speed and its exponential fitting curve (black curve), and (b) load characteristics of PPS-based USM with t5 vibrator.

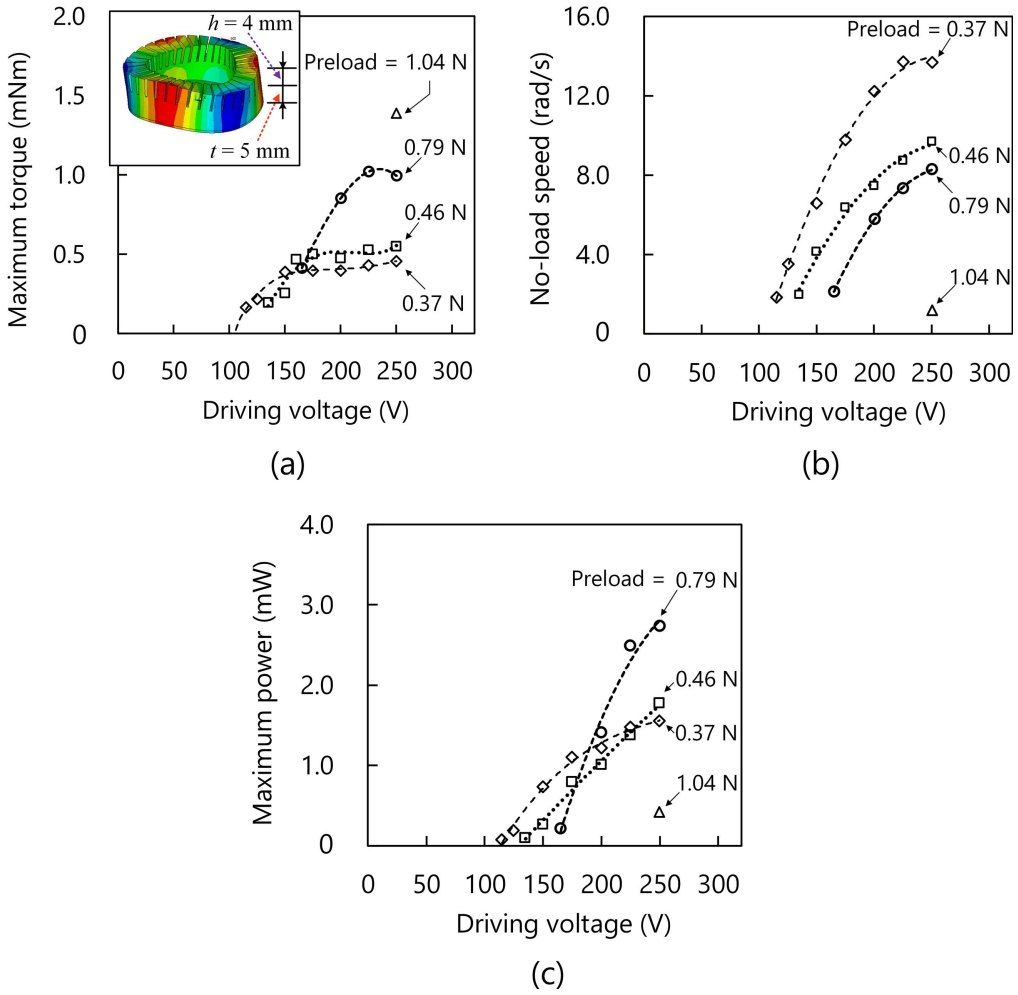

Figure 12. Motor performance with t5 vibrator as a function of driving voltage under different preloads: (a) maximum torque, (b) maximum rotation speed at 250 V, and (c) maximum power.

torque under the optimal preload is suitable for representing the vibrator performance. Figure 12(b) shows that the motor provided its maximum no-load speed when the minimal preload and the maximal voltage are applied to the vibrator. As figure 12(c) shows, at a certain voltage, the output power initially became higher with increasing preload, and then, became lower owing to the rapid reduction in the rotation speed.

Figure 13 shows the motor performance with varying thickness of the un-slotted part at driving voltages of 250 V.

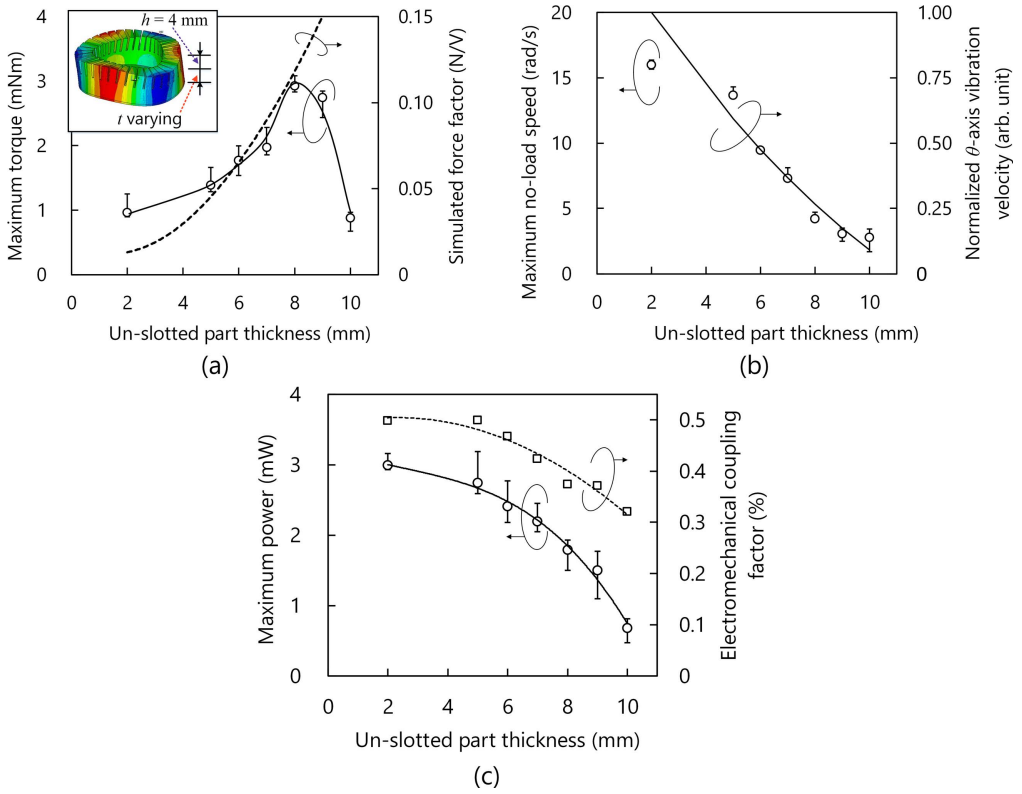

Figure 13. Performance of motors with varying un-slotted part thicknesses. (a) Maximum torques at optimal preloads, (b) maximum no-load rotation speeds, and (c) maximum power when voltages of 250 V were applied.

The performance of each motor was evaluated at random three different positions. Figure 13(a) shows the maximum torques when optimal preloads were applied to the motors. As the un-slotted part thickness increased from 2 to 8 mm, the maximum torque exhibited an increase from approximately 0.9–3.0 mNm. However, the maximum torque decreased from 3.0 to 0.8 mNm when the thickness increased from 8 to 10 mm. Under a certain voltage and a sufficiently high preload, a thicker vibrator generates a higher driving force to the rotor. This is a reason for the increase in the maximum torque when the un-slotted part thickness was varied from 2 to 8 mm. In general, slip exists at contacting surfaces in traveling-wave USMs because there are velocity differences between the vibrator and the rotor along both the θ and r axes [22]. As mentioned above, the θ-axis vibration velocity is parallel to the rotational direction. The points near the crest, which yield higher θ-axis vibration velocities than the rotation speed, accelerates the rotor. Slip is generated on a part of the points with relatively low vibration velocities [7]. In contrast, since the r-axis vibration velocities are vertical to the rotation direction, slip is generated on all contacting points except for those with radial vibration velocities of zero (theoretically, six points with the 3rd bending mode). Besides, the r-axis vibration velocities, particularly in the cases of the thicker vibrators, are higher than the θ-axis vibration velocities (see figure 3(a)). Thus, the frictional loss caused by slip should be dominantly attributed to the r-axis vibration component [23, 24]. As the vibrator becomes thicker, both the force factor and the r-axis vibration velocity increase, and the negative effect on the torque caused by the friction loss offsets the positive effect due to the enhancement in the force factor. Thus, the rapid reduction in the maximum torque in the thickness range from 8 to 10 mm originates from the large increase in the friction loss. To quantitatively estimate the output torque, a simulation model for the friction on the contacting surface between the polymer-based vibrator and the metal rotor should be developed in the future. Since the polymer-based motor has a softer vibrator and a harder rotor, it may provide a friction different from the conventional metal-based motor, of which the vibrator is commonly harder than the rotor [6, 7, 23, 24]. The previous study shows that the conventional metal-based motor with the same diameter yields the highest torque when its un-slotted part thickness is less than 4 mm [7]. Clearly, a thicker vibrator is needed for the PPS-based motor. As figure 13(b) shows, the maximum no-load speed decreased as the vibrator became thicker because the θ-axis vibration velocity was lowered. The maximum power shown in figure 13(c) decreased from 3.0 to 0.8 mW as the un-slotted part thickness ranged from 2 to 10 mm owing to the reduction in electromechanical coupling factor. The friction loss also lowers the output power particularly for the thick vibrators.

Figure 14 shows the performance of motors with varying teeth height. Their un-slotted part thicknesses are 8 mm. The motors with lower teeth height yielded higher output torques. When a preload of 6.4 N was applied to the vibrator with

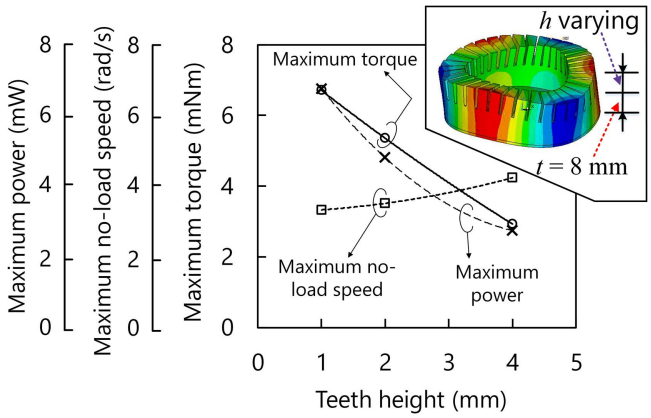

Figure 14. Performance of motors with varying teeth height.

$t = 8$ mm and $h = 1$ mm, the maximum torque at 250 V reached 6.7 mNm, approximately 10 times the value of our previous motor prototype [12]. The maximum no-load speed and the output power became lower and higher, respectively, as the teeth height decreased.

Figures 7 and 8 indicate that it is difficult to significantly increase the output torque by adjusting the slot width w and the inner diameter D_{in} since they are close to the optimal values. Figure 5 indicates that a larger torque can be obtained by using the piezoelectric ceramic elements with thicknesses of less than 0.05 mm or over 1.5 mm. In our experiments, piezoelectric ceramics of less than 0.2 mm in thickness were unavailable because they were easy to fracture[1, 2]. Thin piezoelectric films can be obtained by sputtering and hydrothermal synthesis [20, 25]. However, a large-area piezoelectric film, e.g., a piezoelectric ceramic element with a 30 mm outer diameter used in this study, has not been reported. Besides, it is feasible to enhance the output torque and power by using the piezoelectric ceramic elements with thicknesses of over 1.5 mm, but the USM weight becomes larger as piezoelectric ceramics have much higher densities than PPS. In the future, the optimal thickness of piezoelectric ceramics will be discussed considering the power density (the ratio of output torque to weight) of USM.

5. Discussions: Performance comparison between polymer- and metal-based vibrators

For comparison, we fabricated a stainless-steel-based vibrator with a 4 mm thick un-slotted part and 4 mm high teeth, and glued a 0.1 mm thick PPS film on its top surface to obtain the same friction characteristics as the PPS-based motors. The resonance frequency and the electromechanical coupling factor corresponding to the 3rd bending mode were 25.89 kHz and 4.9%, respectively. At 250 V, its maximum torque and rotation speed were 20.8 mNm and 10.8 rad s^{-1}, respectively, and its maximum output power reached 31.6 mW. Though the vibrator of the PPS-based motor was structurally optimized, its output torque and power were still lower. To explore the reason for the relatively low torque, we compared the vibration velocity ratios and the force factors between the PPS- and metal-based vibrators with the same structures. The material constants of metals are given in table 1. As shown in figure 15(a), there is no observable difference in the ratios v_θ/v_z and v_r/v_z among the vibrators. In contrast, the force factor in figure 15(b) shows a great difference among these materials. For example, the copper-alloy-based vibrator with an 8 mm-thick un-slotted part exhibits a force factor of 0.99 N V^{-1}, higher than those of the stainless-steel-, aluminum-alloy-, and PPS-based vibrators (0.65, 0.60 and 0.12 N V^{-1}, respectively). To obtain a force factor of 0.15 N V^{-1}, the sufficient thickness is 2.5 mm for the copper-alloy-based vibrator and 10 mm for the PPS-based vibrator. Thus, a thicker vibrator is needed for the PPS-based motor to generate a driving force comparable to that of the metal-based motor. Among the tested materials in table 1, the elastic modulus and the density of copper alloy are relatively close to those of piezoelectric ceramics, and the copper-alloy-based vibrator provides a relatively high force factor. In contrast, there is a significant difference in the mechanical constants between the vibrating body and the piezoelectric ceramic element of the PPS-based vibrator, and it may result in the low force factor. Thus, the torque of the PPS-based USM is difficult to significantly enhance by adjusting the dimensions because it is dominantly restricted by low mechanical constants of PPS. In addition, since the thinner vibrators, which have sufficiently high force factor, are used in metal-based motors, their radial vibration components are lower than polymer-based ones. The motors made of other commonly employed functional polymers also face the same problems because they have almost similar elastic moduli and densities [12, 13]. The lower output powers of PPS-based motors originate from their low electromechanical coupling factors, which are lower than 0.1 times the value of the stainless-steel-based vibrator.

6. Conclusion

To enhance the performance of polymer-based USMs, a preliminary investigation on the shape parameters of their vibrators was carried out. Through analytical and experimental explorations, the following conclusions were obtained:

(1) At 250 V, the PPS-based motor with a 30 mm diameter yielded the maximum torque of 6.7 mNm, 10 times the value of our previous polymer-based motor.
(2) Relatively low torques of polymer-based motors are caused by low force factors and undesirable radial vibration components of their vibrators. Relatively low output power is mainly attributed to the low electromechanical coupling factor.

[1] Manual of Fuji Ceramic's products: http://fujicera.co.jp/product/elements/
[2] Manual of APC International Ltd's products: https://americanpiezo.com/product-service/custom-piezoelectric-elements/shapes-sizes.html

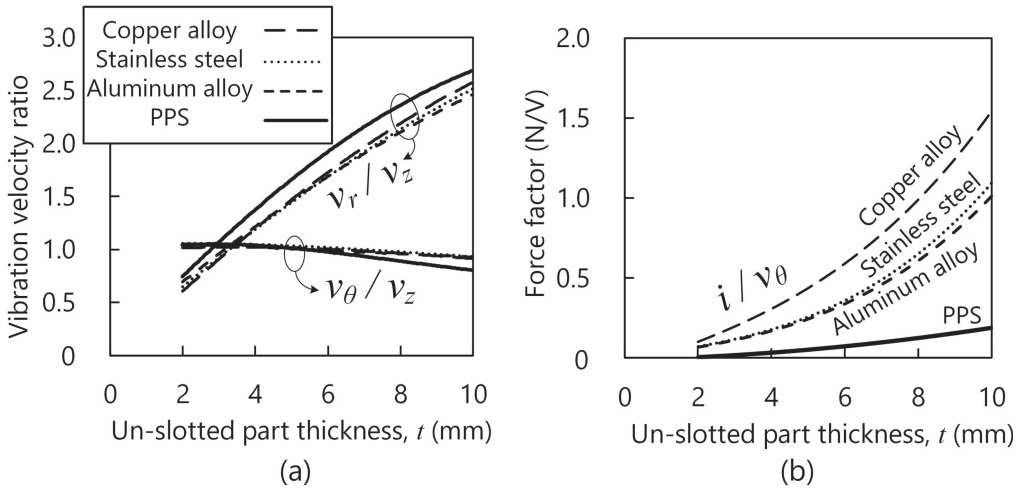

Figure 15. (a) Elliptical motion shapes and (b) force factors of PPS-, stainless-steel-, aluminum-, and copper-alloy-based vibrators.

(3) The low force factor of polymer-based vibrator possibly originates from the difference in the mechanical constants between polymer and piezoelectric ceramics.
(4) Higher high force factor and lower radial vibration component are desirable for not only polymer- but also metal-based cylindrical vibrators.

Though polymer-based motor cannot generate an output torque comparable to those of the commercially available motors, it still has some applications, for example, in the chemical industry because polymer is resistant to acid and alkali [23], or as an actuator in machines where the light-weight is especially required. PPS with a fiber reinforced structure, having a much higher elastic modulus than that of the currently employed PPS [13], is a promising material for enhancing the torque of the polymer-based USM.

Acknowledgments

The authors are indebted to the Daicel Corporation for providing the functional polymers, and the staff members of the Precision and Manufacturing Center, Technical Department, Tokyo Institute of Technology, for machining the motor components used in this study. They also thank Dr Wei Qiu, who is presently with the Department of Physics, Technical University of Denmark, and formerly Laboratory for Future Interdisciplinary Research of Science and Technology, Tokyo Institute of Technology, for the fruitful discussions with him. This work was supported by the Adaptable and Seamless Technology Transfer Program, A-step, Grant Number AS2711904S, from the Japan Science and Technology Agency, JST, and the work of J Wu was supported by a Grant-in-Aid JSPS Research Fellows (No. 17J05057).

ORCID iDs

Jiang Wu https://orcid.org/0000-0002-6899-5601
Yosuke Mizuno https://orcid.org/0000-0002-3362-4720
Kentaro Nakamura https://orcid.org/0000-0003-2899-4484

References

[1] Ueha S and Tomikawa Y 1993 *Ultrasonic Motors—Theory and Applications* (Oxford: University Press)
[2] Nakamura K, Kurosawa M K and Ueha S 1991 Characteristics of a hybrid transducer-type ultrasonic motor *IEEE Trans. Ultrason. Ferroelectr. Freq. Control* **38** 188–93
[3] Hirata H and Ueha S 1995 Design of a traveling wave type ultrasonic motor *IEEE Trans. Ultrason. Ferroelectr. Freq. Control* **42** 225–31
[4] Huang S, Tan K and Lee T 2009 Adaptive sliding-mode control of piezoelectric actuators *IEEE Trans. Ind. Electron.* **56** 3514–22
[5] Zhou X, Chen W and Liu J 2016 Novel 2-DOF planar ultrasonic motor with characteristic of variable mode excitation *IEEE Trans. Ind. Electron.* **63** 6941–8
[6] Morita T, Kurosawa M K and Higuchi T 1998 A cylindrical micro ultrasonic motor using PZT thin film deposited by single process hydrothermal method ($\Phi = 2.4$ mm, $L = 10$ mm stator transducer) *IEEE Trans. Ultrason. Ferroelectr. Freq. Control* **45** 1178–87
[7] Hirata H and Ueha S 1993 Characteristics estimation of a traveling wave type ultrasonic motor *IEEE Trans. Ultrason. Ferroelectr. Freq. Control* **40** 402–6
[8] Chen X, Li X, Chen J and Dong S 2013 A square-plate ultrasonic linear motor operating in two orthogonal first bending modes *IEEE Trans. Ultrason. Ferroelectr. Freq. Control* **60** 115–20
[9] Dong S, Lim S-P, Lee K-H, Zhang J, Lim L-C and Uchino K 1995 Piezoelectric ultrasonic micro motor with 1.5 mm diameter *IEEE Trans. Ultrason. Ferroelectr. Freq. Control* **50** 361–7
[10] Hagood N W and McFarland A J 1995 Modeling of a piezoelectric rotary ultrasonic motor *IEEE Trans. Ultrason. Ferroelectr. Freq. Control* **42** 210–24
[11] Liu Y, Chen W, Liu J and Shi S 2013 A rectangle-type linear ultrasonic motor using longitudinal vibration transducers with four driving feet *IEEE Trans. Ultrason. Ferroelectr. Freq. Control* **60** 777–85
[12] Wu J, Mizuno Y, Tabaru M and Nakamura K 2016 Measurement of mechanical quality factors of polymers in

flexural vibration for high-power ultrasonic application *Ultrasonics* **69** 74–82
[13] Wu J, Mizuno Y, Tabaru M and Nakamura K 2015 Ultrasonic motors with polymer-based vibrators *IEEE Trans. Ultrason. Ferroelectr. Freq. Control* **62** 2169–77
[14] Nakamura K, Kakihara K, Kawakami M and Ueha S 2000 Measuring vibration characteristics at large amplitude region of material for high power ultrasonic vibration system *Ultrasonics* **38** 122–6
[15] Wu J, Mizuno Y, Tabaru M and Nakamura K 2016 Traveling wave ultrasonic motor using polymer-based vibrator *Japan. J. Appl. Phys.* **55** 018001
[16] Kurosawa M and Ueha S 1991 Hybrid transducer type ultrasonic motor *IEEE Trans. Ultrason. Ferroelectr. Freq. Control* **38** 89–92
[17] Graff K F 1991 *Wave Motion in Elastic Solids* (New York: Dover)
[18] Nakamura K, Kurosawa M K, Kurebayashi H and Ueha S 1991 An estimation of load characteristics of an ultrasonic motor by measuring transient responses *IEEE Trans. Ultrason. Ferroelectr. Freq. Control* **38** 481–5
[19] Watson B, Friend J and Yeo L 2009 Piezoelectric ultrasonic resonant motor with stator diameter less than 250 μm *J. Micromech. Microeng.* **19** 022001
[20] Morita T, Kurosawa M K and Higuchi T 2000 A cylinder shaped micro ultrasonic motor utilizing PZT thin film (1.4 mm in diameter and 5.0 mm long stator transducer) *Sensors Actuators* **83** 225–30
[21] Shigematsu T and Kurosawa M K 2008 Friction drive of an SAW motor: I. Measurements *IEEE Trans. Ultrason. Ferroelectr. Freq. Control* **55** 2005–15
[22] Ibrahim R A 1994 Friction-induced vibration chatter, squeal, and chaos: I. Mechanics of contact and friction *Appl. Mech. Rev.* **47** 209–26
[23] Lu X, Hu J and Zhao C 2011 Analyses of the temperature field of traveling-wave rotary ultrasonic motors *IEEE Trans. Ultrason. Ferroelectr. Freq. Control* **58** 2708–19
[24] Wallaschek J 1997 Contact mechanics of piezoelectric ultrasonic motors *Smart Mater. Struct.* **7** 369–81
[25] Muralt P 2000 PZT thin films for micro-sensors and actuators: where do we stand *IEEE Trans. Ultrason. Ferroelectr. Freq. Control* **47** 903–15